A finite-element formulation for room acoustics simulation with microperforated panel sound absorbing structures: Verification with electro-acoustical equivalent circuit theory…

Okuzono, Takeshi

Sakagami, Kimihiro

(Citation)
Applied Acoustics,95:20-26

(Issue Date)
2015-08

(Resource Type)
journal article

(Version)
Accepted Manuscript

(URL)
https://hdl.handle.net/20.500.14094/90003470

A finite-element formulation for room acoustics simulation with microperforated panel sound absorbing structures:Verification with electro-acoustical equivalent circuit theory and wave theory

Takeshi Okuzono[a,1] Kimihiro Sakagami[a]

[a]*Environmental Acoustic Laboratory, Department of Architecture, Graduate School of Engineering, Kobe University, 1-1, Rokkodai-cho, Nada-ku, Kobe-city 657-8501, Japan*

Abstract

A simple frequency-domain finite-element method (FD-FEM) for sound field analyses inside rooms installed with microperforated panel (MPP) sound absorbing structures is described here. This method can also analyze sound absorbing structures composed of MPPs and permeable membranes (PM) simply by changing the only material parameters of MPP into those of PM. As the first stage of the study, the validity of the present FD-FEM is tested through the numerical experiments based on the impedance tube method for measuring the absorption characteristics at normal incidence. In the numerical experiments, we calculated the absorption characteristics of a single MPP absorber, a double-leaf MPP space absorber and a space absorber composed of MPP and PM by using the FD-FEM in two-dimensions, and the computed absorption characteristics are compared with those calculated by an electro-acoustical equivalent circuit theory or a wave theory based on Helmholtz-Kirchhoff boundary integral equation. The results showed that the presented FD-FEM can analyze the absorption characteristics at normal incidence of the MPP sound absorbing structures accurately with the simplicity of the formulation.

Keywords: Room acoustics, Microperforated panel, Finite element

[1]Corresponding author. Tel./fax: +81 78 803 6577.
E-mail address: okuzono@port.kobe-u.ac.jp (T. Okuzono).

method, Frequency domain, Verification

1. Introduction

A microperforated panel (MPP) has been recognized as one of the most promising alternatives of the next-generation sound absorbing materials thanks to the superior material performances in durability, weatherability, recyclability and flexibility of design as well as the attractive broadband sound absorption characteristics. There have been proposed various sound absorbing structures using MPPs and their absorption characteristics were studied theoretically, experimentally and computational experimentally [1, 2, 3, 4, 5, 6, 7, 8, 9, 10, 11]. As the conventional absorbing structure, an MPP is placed in front of a rigid wall with an air-cavity in-between to form the Helmholtz resonator [1]. A double resonator type absorber using two MPPs with a rigid wall is one of the strategies for extending the absorption band to lower frequencies [1]. Space absorbers which consist of multiple leaf MPP without a rigid backing can also be available to offer the much wider absorption frequency range [3, 4]. DLMPP [3] and TLMPP [4] use two or three MPPs without a rigid back wall and offer the wideband sound absorption with additional absorption at low frequencies. MPP-membrane space absorber [5] which consists of an MPP and a permeable membrane without a rigid back wall is a cost-efficient alternative of DLMPP. Practically, these space absorbers can be used as a sound absorbing panel or partition. Also, there proposed light-weight three-dimensional space sound absorbers such as CMSA [6] and RMSA [7] for providing further flexibility in the installation location and in the design. More recently, numerical methods such as computational fluid dynamics (CFD) and finite element method (FEM) have been used to model the MPPs with the consideration of advantage in handling arbitrary geometries [8, 9, 10, 11]. CFD analysis has been used to calculate the acoustic impedance of the MPP having arbitrary hole geometry and to construct more accurate impedance model according to the hole type [8, 9]. An FE model based on a porous material model [10] and a vibroacoustic FEM [11] using plate elements for bending vibration and acoustic impedance for the effect of the micro-perforation have also been presented to model the MPP absorbers with complex configurations.

On the other hand, the development of an accurate computer simulation technique to predict sound fields inside buildings with the above-mentioned

MPP sound absorbing structures is also beneficial for architectural acoustical design as well as the development of more efficient sound absorbing structures using MPP. Because the absorption mechanism of the MPP absorbing structures is based on the Helmholtz resonance, the use of the wave-based method is appropriate to model the MPP than the use of the geometrical method. Recently, wideband wave-based room acoustics simulation up to several kilohertz frequencies is becoming realistic option with the drastic advancements in the computer technology [12, 13]. The authors have also proposed some FEM [14, 15, 16, 17] for conducting the large-scale room acoustics simulation with $\mathcal{O}(10^7)$ degrees of freedom (DOF) efficiently, and the FEM provides more accurate results than conventional methods with the lower computational cost. However, the development of the wave-based method for room acoustics simulation with the MPP sound absorbing structures is still insufficient despite the fact that the MPP sound absorbing structures have received considerable attention. The important point in the development is computationally efficient modeling of the MPP because the wideband wave-based room acoustics simulation is still computationally costly.

In this paper, we propose a mathematically simple and computationally efficient frequency-domain FEM (FD-FEM) for sound field analysis in rooms with the MPP sound absorbing structures, with an emphasis on a practical utility rather than a detailed absorbing modeling. As the first stage of the research, the validity of the FD-FEM using the first order FEs are tested through the numerical experiments based on an impedance tube method for measuring normal incidence sound absorption characteristics. The question in the numerical experiments is whether the presented FEM can analyze absorption characteristics of various MPP absorbing structures. For the purpose, the impedance tube problem is appropriate as one of the benchmark problems because we can use existing theoretical solutions for absorption characteristics at normal incidence of various MPP absorbing structures. In the numerical experiments, as the theoretical solutions, an electro-acoustical equivalent circuit theory with the effect of the sound-induced vibration [18] and a more sophisticated wave theory based on Helmholtz-Kirchhoff boundary integral equation [19] are used to verify the numerical results. First, we describe a theory of the FD-FEM, in which the surface density and the acoustic impedance of the MPP are used as the material parameters. Then, according to the impedance tube method using the transfer function, the surface impedance and the normal incidence absorption coefficient in the above-mentioned conventional absorbing structure are calculated using the

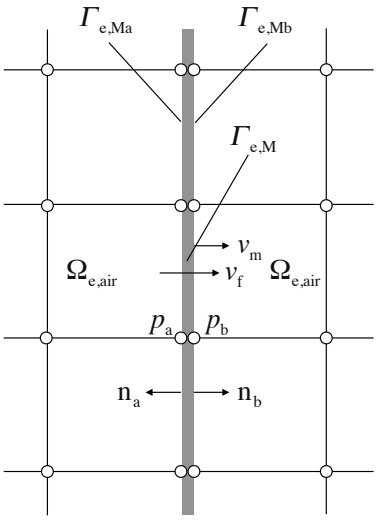

Figure 1: An FE model for MPP.

presented FD-FEM, and the calculated absorption characteristics are compared with those calculated by the electro-acoustical equivalent circuit theory. Finally, the absorption characteristics of a DLMPP and an MPP-PM are calculated using the FD-FEM and compared with those calculated by the wave theory.

2. Theory

According to a formulation of limp membrane elements proposed by Sakuma et al [20], we incorporate the contribution from MPP surfaces into FE equation, in which only the mass of the MPP is considered to include the effect of sound-induced vibration of the material itself, which is important for treating the light weight MPP [18]. Although the presented formulation is mathematically simpler than the above-mentioned FEM such as the FEM based on the porous material model and the vibroacoustic FEM, the application range is restricted than those methods because the effects of bending stiffness and support conditions of the MPP cannot be considered in this formulation.

2.1. Boundary condition of MPP surfaces in FE model

Figure 1 presents an FE model of the MPP in which $\Omega_{e,air}$ and $\Gamma_{e,M}$ represent the air element and the MPP element derived with the contributions

from both boundary surfaces of the MPP $\Gamma_{\mathrm{e,Ma}}$ and $\Gamma_{\mathrm{e,Mb}}$. p_{a} and p_{b} represent the sound pressures at both sides of the MPP. v_{f} and v_{m} represent the average particle velocity over the tube cross-section and vibration velocity of the MPP. $\mathbf{n}_{\mathrm{a}}$ and $\mathbf{n}_{\mathrm{b}}$ are the normal vectors at the boundaries.

In the FE formulation, we derive a discretized matrix equation assuming that the boundary surfaces of the MPP element $\Gamma_{\mathrm{e,Ma}}$ and $\Gamma_{\mathrm{e,Mb}}$ are vibration boundaries, as described below. From the definition of the acoustic impedance Z_{M} of the MPP, v_{f} can be obtained as

$$v_{\mathrm{f}} = \frac{p_{\mathrm{a}} - p_{\mathrm{b}}}{Z_{\mathrm{M}}}. \tag{1}$$

According to Maa's impedance model [1], Z_{M} including the end corrections is approximately given as

$$Z_{\mathrm{M}} = \frac{R_0 + iI_0}{\sigma}, \tag{2}$$

with

$$R_0 = \frac{32\eta t}{d^2}\left(\sqrt{1 + \frac{K^2}{32}} + \frac{\sqrt{2}}{8}K\frac{d}{t}\right), \tag{3}$$

$$I_0 = \rho_0 \omega t\left(1 + \frac{1}{\sqrt{9 + \frac{K^2}{2}}} + 0.85\frac{d}{t}\right), \tag{4}$$

$$K = d\sqrt{\frac{\omega\rho_0}{4\eta}}, \tag{5}$$

where ρ_0, t, d, σ, η, ω, and i respectively represent the air density, the panel thickness, the hole diameter, the perforation ratio, the dynamic viscosity of the air(17.9 μPa s), the angular frequency, and the imaginary unit.

Further, we define the equation of motion of the MPP simply as

$$i\omega M_{\mathrm{MPP}} v_{\mathrm{m}} = p_{\mathrm{a}} - p_{\mathrm{b}}. \tag{6}$$

Here, M_{MPP} is the surface density of the MPP. Assuming the local reaction on the boundaries $\Gamma_{\mathrm{e,Ma}}$ and $\Gamma_{\mathrm{e,Mb}}$, the following vibrating boundary condition for each boundary is given by

$$\frac{\partial p}{\partial n} = \begin{cases} -i\omega\rho_0(v_{\mathrm{m}} + v_{\mathrm{f}}) & \text{on } \Gamma_{\mathrm{e,Ma}}, \\ i\omega\rho_0(v_{\mathrm{m}} + v_{\mathrm{f}}) & \text{on } \Gamma_{\mathrm{e,Mb}}. \end{cases} \tag{7}$$

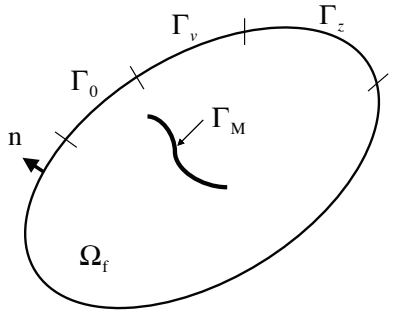

Figure 2: A closed sound field Ω_f with rigid boundary Γ_0, vibration boundary Γ_v, impedance boundary Γ_z, and boundary Γ_M related to MPP.

2.2. FE formulation for three dimensional sound field analysis in rooms with MPP

We consider a closed sound field Ω_f with rigid boundary Γ_0, vibration boundary Γ_v, impedance boundary Γ_z, and boundary Γ_M related to the MPP governed by the wave equation, as shown in Fig. 2. By introducing the FE approximations to sound pressure and weight function in the weak form derived from the wave equation, the discretized matrix equation for the steady state sound field can be obtained as

$$\sum_{\mathrm{e}}^{n_\mathrm{e}}\Bigg[\int_{\Omega_{\mathrm{e,air}}}\nabla \boldsymbol{N}^T\nabla \boldsymbol{N}dV\boldsymbol{p}_\mathrm{e}-k^2\int_{\Omega_{\mathrm{e,air}}}\boldsymbol{N}^T\boldsymbol{N}dV\boldsymbol{p}_\mathrm{e} - \int_{\Gamma_{\mathrm{e},z}+\Gamma_{\mathrm{e,M}}}\boldsymbol{N}^T\frac{\partial p}{\partial n}dA\Bigg]=\sum_{\mathrm{e}}^{n_\mathrm{e}}\int_{\Gamma_{\mathrm{e},v}}\boldsymbol{N}^T\frac{\partial p}{\partial n}dA, \tag{8}$$

where k, $\boldsymbol{N}$, $\boldsymbol{p}_\mathrm{e}$ and n_e respectively represent the wavenumber, the shape function, the nodal sound pressure vector, and the number of FEs. The contributions from both boundary surfaces of the MPP can be considered by substituting the boundary conditions, Eq. (7), into the third term in the left hand side of Eq. (8) as presented below.

$$\int_{\Gamma_{\mathrm{e,M}}}\boldsymbol{N}^T\frac{\partial p}{\partial n}dA=\int_{\Gamma_{\mathrm{e,Ma}}}\boldsymbol{N}^T\frac{\partial p}{\partial n}dA+\int_{\Gamma_{\mathrm{e,Mb}}}\boldsymbol{N}^T\frac{\partial p}{\partial n}dA, \tag{9}$$

where

$$\int_{\Gamma_{\mathrm{e,Ma}}} \boldsymbol{N}^T \frac{\partial p}{\partial n} dA = -(\frac{\rho_0}{M_{\mathrm{MPP}}} + \frac{i\omega\rho_0}{Z_{\mathrm{M}}}) \int_{\Gamma_{\mathrm{e,Ma}}} \boldsymbol{N}_{\mathrm{a}}^T (\boldsymbol{N}_{\mathrm{a}} - \boldsymbol{N}_{\mathrm{b}}) dA \boldsymbol{p}_{\mathrm{e}}, \tag{10}$$

$$\int_{\Gamma_{\mathrm{e,Mb}}} \boldsymbol{N}^T \frac{\partial p}{\partial n} dA = (\frac{\rho_0}{M_{\mathrm{MPP}}} + \frac{i\omega\rho_0}{Z_{\mathrm{M}}}) \int_{\Gamma_{\mathrm{e,Mb}}} \boldsymbol{N}_{\mathrm{b}}^T (\boldsymbol{N}_{\mathrm{a}} - \boldsymbol{N}_{\mathrm{b}}) dA \boldsymbol{p}_{\mathrm{e}}. \tag{11}$$

Here, $\boldsymbol{N}_{\mathrm{a}}$ and $\boldsymbol{N}_{\mathrm{b}}$ represent the shape functions at nodes on $\Gamma_{\mathrm{e,Ma}}$ and $\Gamma_{\mathrm{e,Mb}}$ in which pair of nodes has same function form as shown in the later.

Considering the remaining boundary conditions in term of Γ_0, Γ_v and Γ_z, the discretized matrix equation for sound field Ω_{f} is represented as

$$[\boldsymbol{K} - k^2 \boldsymbol{M} + ik\boldsymbol{C} + \rho_0 \boldsymbol{D}]\boldsymbol{p} = \boldsymbol{f}, \tag{12}$$

where $\boldsymbol{K}$, $\boldsymbol{M}$, $\boldsymbol{C}$ and $\boldsymbol{D}$ respectively represent the global stiffness matrix, the global mass matrix, the global dissipation matrix, and the global matrix related to the contributions of the MPP as described below. $\boldsymbol{p}$ and $\boldsymbol{f}$ are the sound pressure vector and the external force vector, respectively.

$$\boldsymbol{K} = \sum_{\mathrm{e}}^{n_{\mathrm{e}}} \int_{\Omega_{\mathrm{e,air}}} \nabla \boldsymbol{N}^T \nabla \boldsymbol{N} dV, \tag{13}$$

$$\boldsymbol{M} = \sum_{\mathrm{e}}^{n_{\mathrm{e}}} \int_{\Omega_{\mathrm{e,air}}} \boldsymbol{N}^T \boldsymbol{N} dV, \tag{14}$$

$$\boldsymbol{C} = \sum_{\mathrm{e}}^{n_{\mathrm{e}}} \frac{1}{z} \int_{\Gamma_{\mathrm{e},z}} \boldsymbol{N}^T \boldsymbol{N} dA, \tag{15}$$

$$\boldsymbol{D} = \sum_{\mathrm{e}}^{n_{\mathrm{e}}} (\frac{1}{M_{\mathrm{MPP}}} + \frac{i\omega}{Z_{\mathrm{M}}}) [\int_{\Gamma_{\mathrm{e,Ma}}} \boldsymbol{N}_{\mathrm{a}}^T (\boldsymbol{N}_{\mathrm{a}} - \boldsymbol{N}_{\mathrm{b}}) dA - \int_{\Gamma_{\mathrm{e,Mb}}} \boldsymbol{N}_{\mathrm{b}}^T (\boldsymbol{N}_{\mathrm{a}} - \boldsymbol{N}_{\mathrm{b}}) dA]. \tag{16}$$

Here, z is the normalized acoustic impedance on the boundary surfaces. Although the above formulation is described for three dimensional analysis, two dimensional formulation can be obtained by replacing volume integral and

Table 1: Shape function for MPP elements

	i=1	i=2	i=3	i=4
N_i	$\frac{1}{2}(1-\xi)$	$\frac{1}{2}(1-\xi)$	$\frac{1}{2}(1+\xi)$	$\frac{1}{2}(1+\xi)$
$\frac{\partial N_i}{\partial \xi}$	$-\frac{1}{2}$	$-\frac{1}{2}$	$\frac{1}{2}$	$\frac{1}{2}$

area integral with area integral and line integral, respectively. This formulation is advantageous for large-scale analyses such as the room acoustics simulation because the coefficient matrix of the linear system of equations of Eq. (12) becomes a complex symmetric matrix – a non-Hermitian – with sparsity, which can be expected to be solved by a proper Krylov subspace iterative method for the large-scale analysis. As a reference, when the eight node hexahedral elements and the four node quadrilateral elements are respectively used for spatial discretization in three and two dimensional analyses, the maximum number of nonzero elements of a row in the coefficient matrix of Eq. (12) are only 27 and 9, respectively. Using these FEs, a sparse matrix storage format and Conjugate Orthogonal Conjugate Gradient (COCG) method [21] as a Krylov subspace iterative method, the required memory, RM, for three and two dimensional analyses can be estimated using

$$RM \approx a \cdot DOF \text{ [Bytes]}, \tag{17}$$

where a represents constant. For three and two dimensional analyses, the constant is 672 and 312, respectively. In this estimation, Complex*16 variable is used for storing the coefficient matrix, $\boldsymbol{p}$, $\boldsymbol{f}$ and other vectors for work space in Eq. (12). Integer*4 variable is also used to store the information of the nodal positions of matrix components for sparse matrix-vector products, which is the main numerical operation of the presented FD-FEM. Figure 3 shows the relationship between DOF and RM in three and two dimensional analyses. As an example, using a PC with 8 GByte memory, one can predict a sound field with about 12,000,000 DOF and 25,600,000 DOF in three and two dimensional analyses, respectively.

2.3. Four-node quadrilateral MPP elements for two dimensional analysis

Under the nodal location presented in Fig. 4, the first order four-node quadrilateral MPP elements $\boldsymbol{D}_{\mathrm{e}}$ is derived for two dimensional sound field analysis. Table 1 lists the shape function for the elements where the same

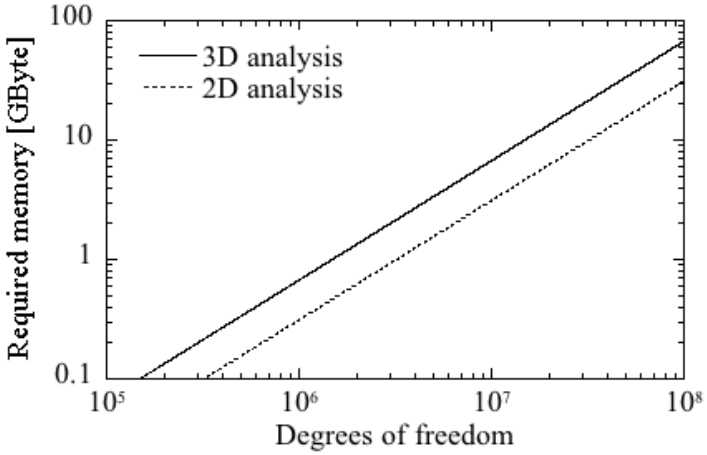

Figure 3: Relationship between degrees of freedom and required memory for three and two dimensional analyses.

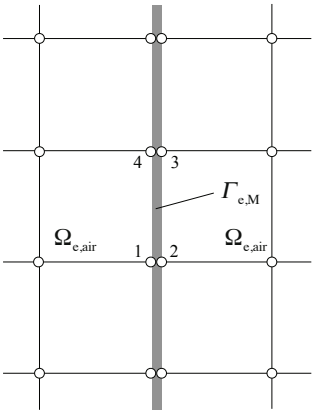

Figure 4: Element node number in a four-node quadrilateral MPP elements.

function as the air elements is used. As mentioned previously, a pair of nodes has the same function form. Using the one dimensional Gauss quadrature rule with two integration points, $\boldsymbol{D}_{\mathrm{e}}$ constructing the global matrix $\boldsymbol{D}$ of Eq. (16) can be calculated as

$$\boldsymbol{D}_{\mathrm{e}} = \left(\frac{1}{M_{\mathrm{MPP}}} + \frac{i\omega}{Z_{\mathrm{M}}}\right) \times \frac{l_{\mathrm{e}}}{6} \begin{bmatrix} 2 & -2 & -1 & 1 \\ -2 & 2 & 1 & -1 \\ -1 & 1 & 2 & -2 \\ 1 & -1 & -2 & 2 \end{bmatrix}, \tag{18}$$

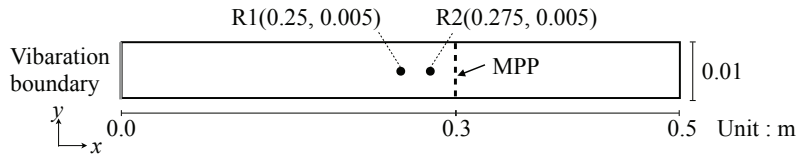

Figure 5: Two dimensional tube model for FE analysis with the conventional sound absorbing structure using an MPP.

where l_{e} is the length of an element. In the Eq. (17), the limp membrane elements [20] for treating membrane materials can be defined simply by replacing M_{MPP} and Z_{M} of the MPP with the surface density M_{PM} and the flow resistance R of the membrane PM. Therefore, presented formulation can handle sound absorbing structures using an MPP and a PM simply by changing only the parameters of the material. The discretized matrix equation for sound field analysis with sound absorbing structure using both MPP and PM can be given as

$$[\boldsymbol{K} - k^2\boldsymbol{M} + ik\boldsymbol{C} + \rho_0\boldsymbol{D} + \rho_0\boldsymbol{L}]\boldsymbol{p} = \boldsymbol{f}, \tag{19}$$

where $\boldsymbol{L}$ is the global matrix of the limp membrane element matrix $\boldsymbol{L}_{\mathrm{e}}$. For two dimensional analysis, $\boldsymbol{L}_{\mathrm{e}}$ is given as

$$\boldsymbol{L}_{\mathrm{e}} = \left(\frac{1}{M_{\mathrm{PM}}} + \frac{i\omega}{R}\right) \times \frac{l_{\mathrm{e}}}{6} \begin{bmatrix} 2 & -2 & -1 & 1 \\ -2 & 2 & 1 & -1 \\ -1 & 1 & 2 & -2 \\ 1 & -1 & -2 & 2 \end{bmatrix}. \tag{20}$$

3. Verification with electro-acoustical equivalent circuit theory

To confirm the validity of the presented FD-FEM, we performed numerical experiments based on the impedance tube method for a single MPP absorber. Figure 5 shows an impedance tube model for two dimensional FE analysis, where an MPP with the following material parameters (d=0.5 mm, t=0.5 mm and σ=0.785%) was placed in front of a rigid wall with an air cavity of 0.2 m thickness. According to the transfer function method using two microphones, the sound pressures at two receiving points R1 and R2 were calculated using the presented FD-FEM to further compute the surface impedance z_0 and the normal incidence absorption coefficient α_0, and the

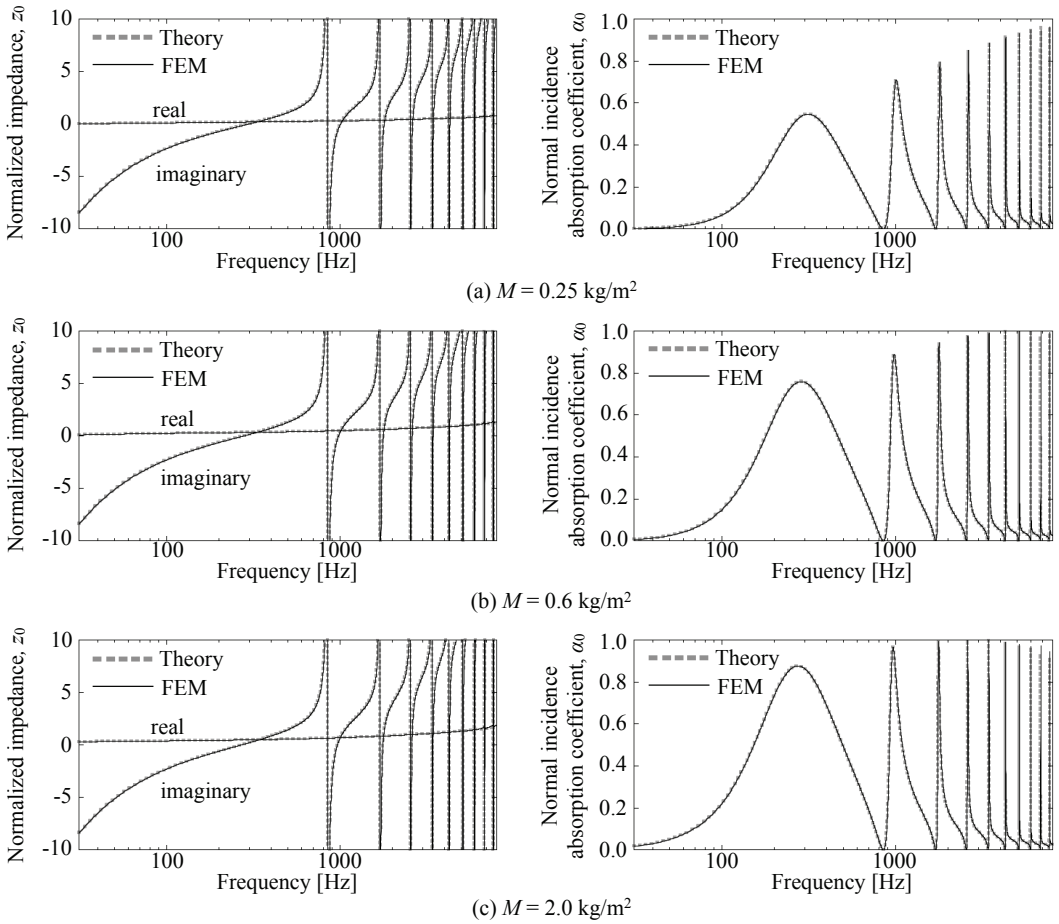

Figure 6: Comparisons of absorption characteristics (z_0 in left and α_0 in right) obtained from FE analysis and equivalent circuit theory for different surface density: (a) 0.25 kg/m^2, (b) 0.6 kg/m^2 and (c) 2.0 kg/m^2. Thick chained line: Theory; solid line: FEM. The both lines in z_0 and α_0 are overlapped well.

computed absorption characteristics were compared with theoretical values by the electro-acoustical equivalent circuit theory [18]. Three surface densities with 0.25, 0.6 and 2.0 kg/m^2 were considered to confirm the effect of the sound-induced vibration of the MPP itself.

In the FE analysis, the sound pressures were calculated at frequencies of 30 Hz to 8 kHz with 1 Hz interval, in which the speed of sound c_0= 340 m/s and ρ_0=1.2 kg/m^3 were assumed, respectively. Vibration velocities of 1.0 m/s were given on the surface in the left-hand side of the tube end,

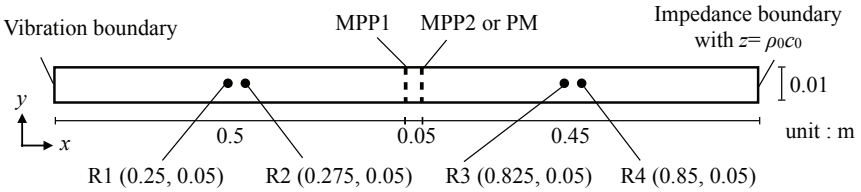

Figure 7: Two dimensional tube model for calculating α_0 and τ_0 of DLMPP and MPP-PM.

and remaining boundaries were assumed to be rigid. Acoustic FEs $\Omega_{\mathrm{e,air}}$ used here were four-node quadrilateral elements with modified integration rules to reduce the dispersion error [22]. An FE mesh was created with 200 elements ($\Omega_{\mathrm{e,air}}$: 198 FEs, and $\Gamma_{\mathrm{e,M}}$: 2 FEs), in which the spatial resolution λ/d_{e} of the mesh was 4.25, where λ and d_{e} respectively represent the wavelength at the upper limit frequency and the maximum nodal distance of an element. COCG method with the absolute diagonal scaling preconditioning was used to solve the linear system of the equations of Eq. (12). Here, a convergence tolerance of 10^{-6}, which determines the resulting accuracy of the solution, was used for the stopping criterion.

Figure 6(a)$\sim$(c) respectively present comparisons of z_0 and α_0 obtained by the FD-FEM and the equivalent circuit theory for the case with different surface densities of the MPP, where the z_0s and α_0s calculated by the FD-FEM are in good agreement with those theoretical values regardless of surface density values. Further, in the comparisons of α_0, the results obtained by the FE analysis capture well a tendency of the theoretical value that lighter MPP show a lower peak at slightly higher frequencies [18].

4. Verification with wave theory

To further confirm the validity of the presented FD-FEM for more complicated sound absorbing structures such as multiple-leaf MPP space absorbers, numerical experiments based on the impedance tube method were again conducted.

4.1. DLMPP

Figure 7 shows a two-dimensional tube model for calculating the absorption characteristics of the DLMPP by the FD-FEM where two MPPs were placed in parallel with an air cavity of 50 mm thickness in-between. The normal incidence absorption coefficient and transmission coefficient, α_0 and

τ_0, were respectively calculated according to the impedance tube method with four microphones, and the difference $\alpha_0 - \tau_0$ between α_0 and τ_0 was further calculated to evaluate the absorptivity of the system, because the DLMPP is a space absorber without a rigid backing. The wave theory based on Helmholtz-Kirchhoff boundary integral equation [19] was used to calculate the theoretical value of $\alpha_0 - \tau_0$ of the DLMPP instead of the electro-acoustical equivalent circuit theory

The material parameters of the two MPPs were assumed to be the same and the following two conditions were assumed. (1)Cond.1 : d=0.15 mm, t=0.4 mm, σ=1.5 %, M_{MPP}=3.0 kg/m^2, and (2)Cond.2 : d=0.2 mm, t=0.2 mm, σ=0.785 %, M_{MPP}=0.12 kg/m^2. In the FE analysis, the sound pressures at four receiving points R1∼R4 were calculated at frequencies of 30 Hz∼5.6 kHz with 5 Hz interval. Vibration velocities of 1.0 m/s were given on the surface in the left-hand side of the tube end, and the characteristic impedance of the air $\rho_0 c_0$ was given for opposite side of the tube end to realize the perfect absorbing condition. The remaining boundaries were assumed to be rigid. 396 acoustic FEs and 4 MPP FEs were used for spatial discretization and the spatial resolution λ/d_{e} of the FE mesh is 6.07. Other settings are the same as the previous section.

Figure 8(a) and (b) show the comparisons of α_0, τ_0 and $\alpha_0 - \tau_0$ obtained by the FE analysis and the wave theory for both conditions, in which the α_0, τ_0 and $\alpha_0 - \tau_0$ by the FE analysis agree well with respective theoretical values, regardless of the conditions. It is also confirmed that lighter MPP has smaller energy dissipation ratio at low frequencies with larger τ_0.

4.2. MPP-permeable membrane absorber

The α_0, τ_0 and $\alpha_0 - \tau_0$ of a space absorber composed of an MPP and a permeable membrane (MPP-PM) were calculated by the FD-FEM to further show the effectiveness of the presented formulation, and the computed absorption characteristics were compared with the theoretical values by the wave theory. Same impedance tube model as shown in Fig. 7 was used for the FE analysis, but the MPP2 was replaced with the permeable membrane having the material parameters of flow resistance R= 816 Pa s/m and the surface density M_{PM}= 3.0 kg/m^2. The material parameters of MPP1 were d=0.15 mm, t=0.4 mm, σ=1.5 %, M_{MPP}=3.0 kg/m^2, respectively. The other settings of the FE analysis were the same as those in the DLMPP. Although the absorption characteristics differ in the cases where the sound is incident

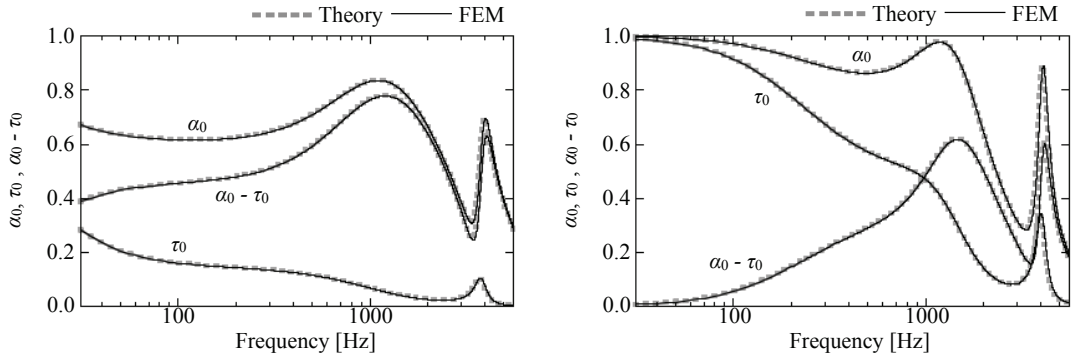

Figure 8: Comparisons of α_0, τ_0 and $\alpha_0 - \tau_0$ of DLMPP obtained from FE analysis and the wave theory: (a) Cond. 1 and (b) Cond. 2. Thick chained line: Theory; solid line: FEM. The both lines are overlapped well.

from the MPP side or the PM side, we assumed here the incidence from the MPP side.

Figure 9 shows a comparison of α_0, τ_0 and $\alpha_0 - \tau_0$ obtained from the FD-FEM and the wave theory where the good agreement can be found between the FEM and the theory. Result showed that the presented formulation can handle the sound absorbing structure composed of the MPP and the PM easily.

Finally, the computational cost of the presented formulation can be considered to be low because almost the same accurate result as the theoretical values were obtained by the FE mesh having only hundreds first order FEs with a dispersion reduction technique. As a reference, the required memory and the computational time for the numerical example of MPP-PM are, respectively, 0.18 MB and 3.8 s with a serial computation on a PC(Windows 7, Intel Core-i7-4770K, 3.5GHz). The COCG method converged with the mean iteration number of 245.7.

5. Conclusions

This paper presented an easy-to-use FD-FEM for room acoustics simulation with the MPP sound absorbing structures, in which MPP's surface density and MPP's acoustic impedance determined by Maa model are used as the material parameters. Because the resulting linear system of equations

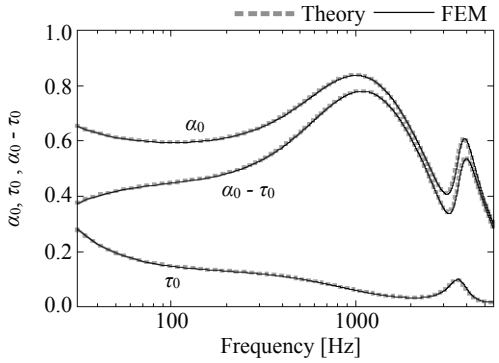

Figure 9: Comparisons of α_0, τ_0 and $\alpha_0 - \tau_0$ of MPP-PM obtained from FE analysis and the wave theory. Thick chained line: Theory; solid line: FEM. The both lines are overlapped well.

of the FD-FEM has a coefficient matrix with complex symmetric sparse matrix, it is suitable for large-scale analysis. As the first stage of the research, the validity of the presented FD-FEM using the first order FEs was tested through the numerical simulations based on the impedance tube method for measuring absorption characteristics at normal incidence. In the numerical simulations using the two-dimensional FE analysis, absorption characteristics of a single MPP absorbing structure and two MPP space absorbers, i.e., DLMPP and MPP-PM, were calculated and compared with those calculated by the electro-acoustical equivalent circuit theory and the wave theory. Numerical results showed that the FD-FEM with a dispersion reduction technique can analyze normal incidence sound absorption characteristics of the sound absorbing structures composed of MPPs and PMs accurately. Further advantage of this FD-FEM is that the limp membrane FEs for treating membrane absorbing structures can be defined simply by changing the only material parameters of MPP into those of permeable membrane. The extension of the FD-FEM to three dimensional problems are the subjects of future research.

Acknowledgment

The work presented in this paper was in part supported by the research grant from NIKKO CO.,LTD.

References

[1] D. Y. Maa, Microperforated-panel wideband absorbers, Noise Control Eng J 1987;29(3):77–84.

[2] D. Y. Maa, Potential of microperforated panel absorber, J Acoust Soc Am 1998;104(5):2861–66.

[3] K. Sakagami, M. Morimoto, W. Koike, A numerical study of double-leaf microperforated panel absorbers, Appl Acoust 2006;67:609–19.

[4] K. Sakagami, M. Yairi, M. Morimoto, Multiple-leaf sound absorbers with microperfrated panels:An overview, Acoust Australia 2010;38(2):76–81.

[5] K. Sakagami, T. Nakamori, M. Morimoto, M. Yairi, Absorption characteristics of a space absorber using a microperforated panel and a permeable membrane, Acoust Sci and Tech 2011;32(1):47–9.

[6] K. Sakagami, T. Oshitani, M. Yairi, E. Toyoda, M. Morimoto, An experimental study on a cylindrical microperforated panel space sound absorber, Noise Control Eng J 2012;60(1):22–8.

[7] K. Sakagami, M. Yairi, E. Toyoda, M. Toyoda, An experimental study on the sound absorption of three-dimensional MPP space sound absorbers: rectangular MPP space sound absorber(RMSA), Acoust Australia 2013;41(2):156–59.

[8] J. S. Bolton, N. Kim, Use of CFD to calculate the dynamic resistive end correction for microperforated materials, Acoust Australia 2010;38(3):134–39.

[9] T. Herdtle, J. S. Bolton, N. N. Kim, J. H. Alexander, R. W. Gerdes, Transfer impedance of microperforated materials with tapered holes, J Acoust Soc Am 2013;134(6):4752–62.

[10] K. Hou, J. S. Bolton, Finite element models for micro-perforated panels, In: Proc inter·noise 2009 on CD-ROM(No.499);2009.

[11] C. Wang, L. Huang, On the acoustic properties of parallel arrangement of multiple micro-perforated panel absorbers with different cavity depths, J Acoust Soc Am 2011;130(1):208–18.

[12] S. Sakamoto, H. Nagatomo, A. Ushiyama , H. Tachibana, Calculation of impulse responses and acoustic parameters in a hall by the finite-difference time-domain method, Acoust Sci and Tech 2008;29(4):256–65.

[13] T. Otsuru, T. Okuzono, R. Tomiku, K. Asniawaty, Large-scale finite element sound field analysis of rooms using a practical boundary modeling technique, In: Proc 19th international congress on sound and vibration 2012 on CD-ROM(No.632);2012.

[14] T. Okuzono, T. Otsuru, R. Tomiku, N. Okamoto, Fundamental accuracy of time domain finite element method for sound-field analysis of rooms, Appl Acoust 2010;71(10):940–6.

[15] T. Okuzono, T. Otsuru, R. Tomiku, N. Okamoto, Application of modified integration rule to time-domain finite-element acoustic simulation of rooms, J Acoust Soc Am 2012;132(2):804–13.

[16] T. Okuzono, T. Otsuru, R. Tomiku, N. Okamoto, Dispersion-reduced spline acoustic finite elements for frequency-domain analysis, Acoust Sci and Tech 2013;34(3):221–4.

[17] T. Okuzono, T. Otsuru, R. Tomiku, N. Okamoto, A finite-element method using dispersion reduced spline elements for room acoustics simulation, Appl Acoust 2014;79:1–8.

[18] K. Sakagami, M. Morimoto, M. Yairi, A note on the effect of vibration of a microperforated panel on its sound absorption characteristics, Acoust Sci and Tech 2005;26(2):204–7.

[19] K. Sakagami, T. Nakamori, M. Morimoto, M. Yairi, Double-leaf microperforated panel space absorbers: A revised theory and detailed analysis, Appl Acoust 2009;70:703–9.

[20] T. Sakuma, T. Iwase, M. Yasuoka, Prediction of sound fields in rooms with membrane materials-Development of a limp membrane element in acoustical FEM analysis and its application-, J Archit Plann Environ Eng 1998;505:1–8.

[21] van der Vorst HA, Melissen J, A Petrov-Galerkin type method for solving $Ax{=}b$, where A is symmetric complex, IEEE Trans Magn 1990;26(2):706–8.

[22] MN Guddati, B Yue, Modified integration rules for reducing dispersion error in finite element methods, Comput Methods Appl Mech Engrg 2004;193:275–87.